Nonvolatile Memory Device Using Gold Nanoparticles Covalently Bound to Reduced Graphene Oxide

Peng Cui, Sohyeon Seo, Junghyun Lee, Luyang Wang, Eunkyo Lee, Misook Min, and Hyoyoung Lee*

Department of Chemistry, National Creative Research Initiative, Center for Smart Molecular Memory, Samsung-SKKU Graphene Center, Sungkyunkwan University, 300 Cheoncheon-Dong, Jangan-Gu, Suwon, Gyeonggi-Do 440-746, Republic of Korea

ABSTRACT Nonvolatile memory devices using gold nanoparticles (AuNPs) and reduced graphene oxide (rGO) sheets were fabricated in both horizontal and vertical structures. The horizontal memory device, in which a singly and doubly overlayered semiconducting rGO channel was formed by simply using a spin-casting technique to connect two gold electrodes, was designed for understanding the origin of charging effects. AuNPs were chemically bound to the rGO channel through a π-conjugated molecular linker. The π-conjugated bifunctional molecular linker, 4-mercapto-benzenediazonium tetrafluoroborate (MBDT) salt, was newly synthesized and used as a molecular bridge to connect the AuNPs and rGOs. By using a self-assembly technique, the diazonium functional group of the MBDT molecular linker was spontaneously immobilized on the rGOs. Then, the monolayered AuNPs working as capacitors were covalently connected to the thiol groups of the MBDT molecules, which were attached to rGOs (AuNP-frGO). These covalent bonds were confirmed by XPS analyses. The current–voltage characteristics of both the horizontal and vertical AuNP-frGO memory devices showed noticeable nonlinear hysteresis, stable write–multiple read–erase–multiple read cycles over 1000 s, and a long retention time over 700 s. In addition, the vertical AuNP-frGO memory device showed a large current ON/OFF ratio and high stability.

KEYWORDS: reduced graphene oxide · self-assembled monolayer · gold nanoparticle · nonvolatile memory · nanotechnology

Graphene, a novel two-dimensional material with an atomic thickness, has attracted much attention due to its fascinating physical and electrical properties, such as giant carrier mobility.[1−8] To produce graphene, several methods such as physical exfoliation and chemical vapor deposition (CVD) have been reported. However, manageable methods for mass production of graphene are still needed to overcome low yield and high cost problems. Recently, chemically reduced graphene oxide nanoplatelets (rGOs), which have semiconducting properties, have been synthesized to avoid the problems that arise during the mass production of graphene. There are many methods for oxidizing graphite into graphene oxide nanosheets (GOs)[9−11] and likewise for reducing GOs into high-quality rGOs.[12,13] According to electronic properties, singly and doubly overlayered rGO layers behave as a semiconductor, and even the thicker rGO films behave as a semimetal.[14] Furthermore, the thin-film rGOs possess a low sheet resistance and a high transparence.[15] Such semiconducting rGOs can be applicable for use as an active component in memory devices. For example, combining graphene (or GOs and rGOs) and gold nanoparticles (AuNPs) through a physical absorption process has been attempted for memory applications.[16,17] In fact, nonvolatile memory behavior has frequently been achieved by charge trapping on the metal nanoparticles embedded in the organic layers.[18] Distribution of AuNPs into thick organic layers has been shown to affect the memory ability of the device. However, memory devices using AuNPs physically embedded in the organic layer or placed on the surface have not been stable due to the relatively unrestrained mobility of the AuNPs, which has resulted in shortened device lifetimes. To make matters worse, in the memory devices where AuNPs were embedded in polymeric or organic thick films, the origin of the charging effect was not clear since the effect may have come from the AuNPs, the organic layer, or both of them.

On the other hand, a nanometer-sized, horizontally structured device with chemically immobilized, monolayered AuNPs on the semiconducting rGO channel is preferable to the previously reported devices of AuNPs-embedded organic thick films for sensing any minute charging effects from the AuNPs. This new device system can provide a clearer understanding for the origin of the charging effect in AuNPs-organic memory devices. The two-dimensional semiconducting rGO channel, fabricated using a simple and inexpensive spin-coating technique, is employed to support the AuNPs, leading to effective control of the transport of charge carriers. Until now, however, owing to the difficulty of forming

* Address correspondence to hyoyoung@skku.edu.

Received for review December 31, 2010 and accepted August 15, 2011.

Published online August 15, 2011
10.1021/nn2021875

chemical bonds between AuNPs and graphene, which has no chemical reactivity, no study of AuNPs covalently bound to graphene (or GOs and rGOs) for memory applications has been reported. For the formation of the covalent binding of AuNPs and graphene, a new material consisting of a bridge molecule (*i.e.*, the molecular linker, which produces the chemical bonds between the AuNPs and the rGO) and a matrix platform (*i.e.*, the rGO sheets) is suggested. In this new system, AuNPs can molecularly link to rGOs and can potentially provide controllable transport within memory devices. In fact, several advantages arise when using the rGO channel, instead of a polymer matrix, as the important constituent element of AuNPs-embedded memory devices: (1) As a highly sensitive semiconducting material, the rGO has good hole and electron mobility. Thus, the rGO can act as both sensor and transducer for the charging and discharging of electrons onto the AuNPs and as a matrix for the active memory layer. (2) The rGO sheet provides covalent anchoring sites for the single-layered molecular linkers. Other polymers and solid materials cannot provide these anchoring sites, making single layer alignment of AuNPs even more difficult. (3) As an ultrathin platform for a bottom-up fabrication, a GO aqueous solution can form an ultrathin (<3 nm) channel, which can then be reduced into the rGO semiconducting channel. The controlled thickness, length, and width of the rGO channel formed between two electrodes can facilitate homogeneous immobilization of the linker molecules and the AuNPs, allowing for further fabrication steps.

Herein, we report a new nonvolatile memory horizontal device composed of monolayered AuNPs chemically bound to rGO sheets through a π-conjugated molecular linker. 4-Mercapto-benzenediazonium tetrafluoroborate (MBDT) salt as a molecular linker was designed to have bifunctional groups: one end group is a diazonium salt that can be chemically connected to rGOs, while the other is a thiol group that can spontaneously anchor to AuNPs. To transport the accumulated and/or polarizable charges onto the AuNPs, the simplest π-conjugated aromatic group, phenyl, was chosen as a communicative wire. Since the MBDT molecular linker between the rGO channel and the AuNPs is expected to provide an energy barrier, the charge carriers of AuNPs can be stayed for some time, leading to nonlinear current−voltage ($I-V$) hysteresis and a long retention time. For the horizontally structured device, singly and doubly overlayered rGOs were chosen for the semiconducting transport channel of charge carriers between two gold electrodes. Then the rGO channel was functionalized with the MBDT molecular linker to create functionalized rGOs (frGOs). It is expected that the resulting rGO channel has sufficient sensitivity to detect the charging/discharging of the monolayered AuNPs. Furthermore, it is anticipated that the rGO channel provides anchoring sites for the bifunctional molecular linkers so that the MBDT molecules can easily form a monolayer on the rGO. In addition, for the vertically structured device, the bulk AuNP-capped MBDT-functionalized rGOs (AuNP-frGOs) were also used for charge transport and storage. The vertically structured device (*e.g.*, metal/insulator/metal (MIM) configuration) with an AuNP-frGOs layer is expected to exhibit large hysteresis and good memory properties for the realization of organic semiconducting memory devices.

RESULTS AND DISCUSSION

Figure 1 shows a schematic of the fabrication process to make these two-type devices of AuNP-frGOs. For the horizontal device, singly and doubly layered GOs were formed by spin-casting on a SiO_2 substrate prepatterned with gold electrodes. Well-dispersed single GOs in water were prepared according to previous reports.[19] The GOs on the device were chemically reduced with hydrazine vapor (Figure 1a). The functionalization of the MBDT molecules to the rGO was achieved by using a self-assembly technique, leading to a thiol-terminated surface on the rGO device (Figure 1b). In the final step, AuNPs were spontaneously immobilized onto the thiol-functionalized rGO device in solution, yielding an AuNP-frGO device (Figure 1c). In addition to the fabrication of the horizontal device, the vertically structured device was prepared as shown in Figure 1d, which was composed of the AuNP-frGOs hybrid material as the active layer between the two electrodes. The active layer was spin-casted onto the bottom electrode (i.e., indium tin oxide, ITO) by using AuNP-frGOs dispersed in dimethylformamide (DMF). An aluminum top-electrode (200 nm thick) was then vapor-deposited onto the active layer (AuNP-frGOs, 50 nm thick) (*i.e.*, Al/AuNP-frGOs/ITO).

For chemical and surface characterization of the AuNP-frGO on the devices, X-ray photoelectron spectroscopy (XPS), atomic force microscopy (AFM), and Raman spectroscopy were employed. Figure 2 shows the XPS surface characterizations for each step. In the XPS spectra of bare rGO samples for the C1s region, the C−O peaks decreased significantly (Figure 2a) when compared with those of GO (Figure 2c), indicating a successful reduction.[20] A carbon skeleton with several oxygen functional groups appeared as a broad shoulder peak of the C−C peak (284.438 eV), showing different binding energies (BE) of 285.675 eV (C−O), and 287.109 eV (C═O) (Figure 2a).[20] Several small oxygen groups remained on the rGO, which were consistent with the previous results of chemically reduced GO.[12,21] After chemical reduction, the thickness of a single rGO sheet was measured as ~0.8 nm[22] (inset of Figure 3a) in a topographical AFM image, which is smaller than that of the single GO sheet (1.0−1.4 nm)[23] due to the removal of oxygen groups from the GO. In particular, an increase in the D peak of the rGO formed at 1350 cm^{-1} from the Raman spectroscopy revealed

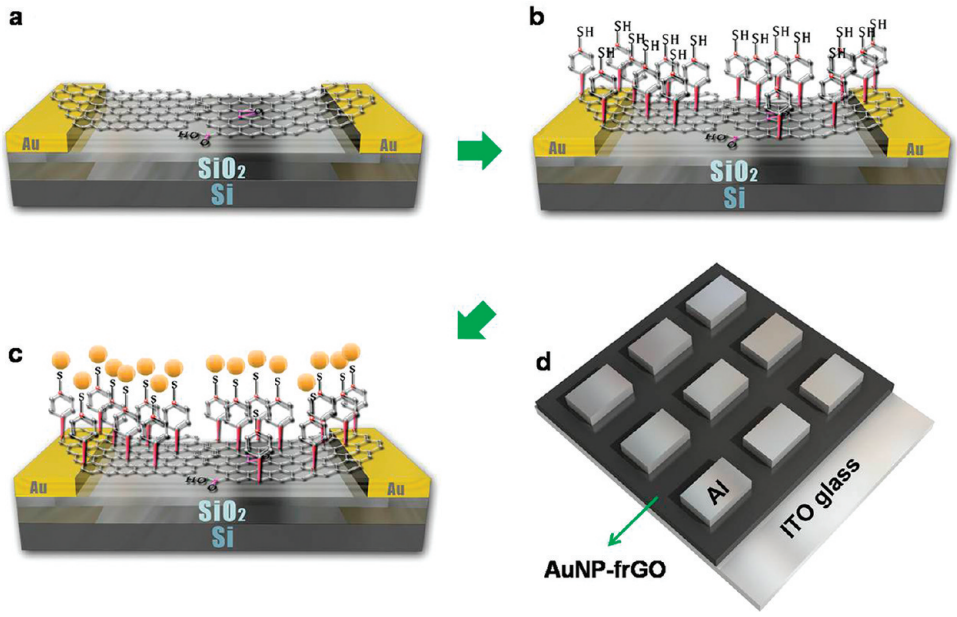

Figure 1. Schematic of the fabrication process for the AuNPs-frGO memory devices: (a–c) An AuNPs-frGO horizontal device was prepared by rGO deposition on the SiO_2 surface between two gold electrodes (a), functionalization of rGO with MBDT (*i.e.*, frGO) (b), and attachment of Au nanoparticles (*i.e.*, AuNPs-frGO) (c). (d) A vertically structured device was prepared by spin-coating the synthesized AuNPs-frGOs (see experimental method section for details) onto an ITO glass substrate and then vapor depositing Al onto the top layer to create Al/AuNPs-frGOs/ITO.

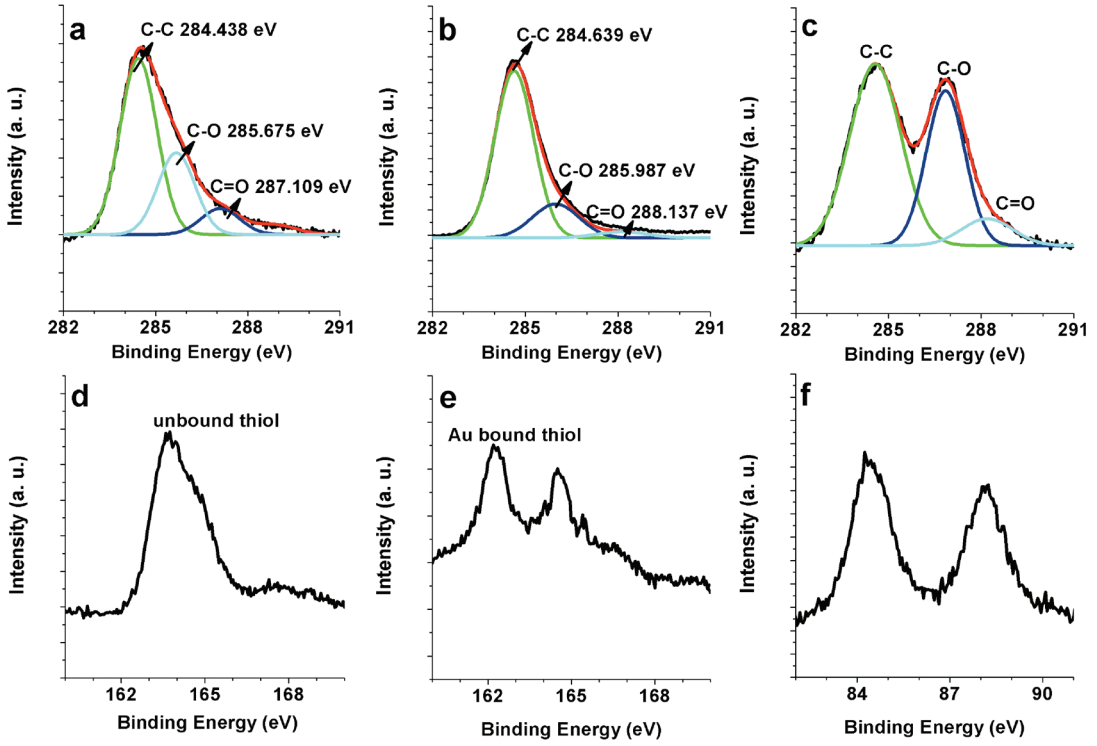

Figure 2. XPS spectra for chemical analysis of GO and rGO sheets in devices during the each fabrication step: (a–c) C1s region of rGO (a), frGO (b), and GO (c). (d,e) S2p region of frGO (d) and AuNP-frGO (e). (f) Au4f region of AuNP-frGO.

a strong increase in the defect density, which is a response of the defunctionalized epoxide and hydroxyl groups after chemical reduction. This process resulted in the formation of sp^3 C–C bonds in the basal plane of the rGOs (Figure 3b).[12,24,25] The rGO pieces were overlapped, single layer by single layer, to form a channel and were successfully connected to two gold electrodes with a gap of 5 μm (Figure 3a). It is assumed that singly or doubly interconnected GO layers are formed in response to repulsive electrostatic interactions

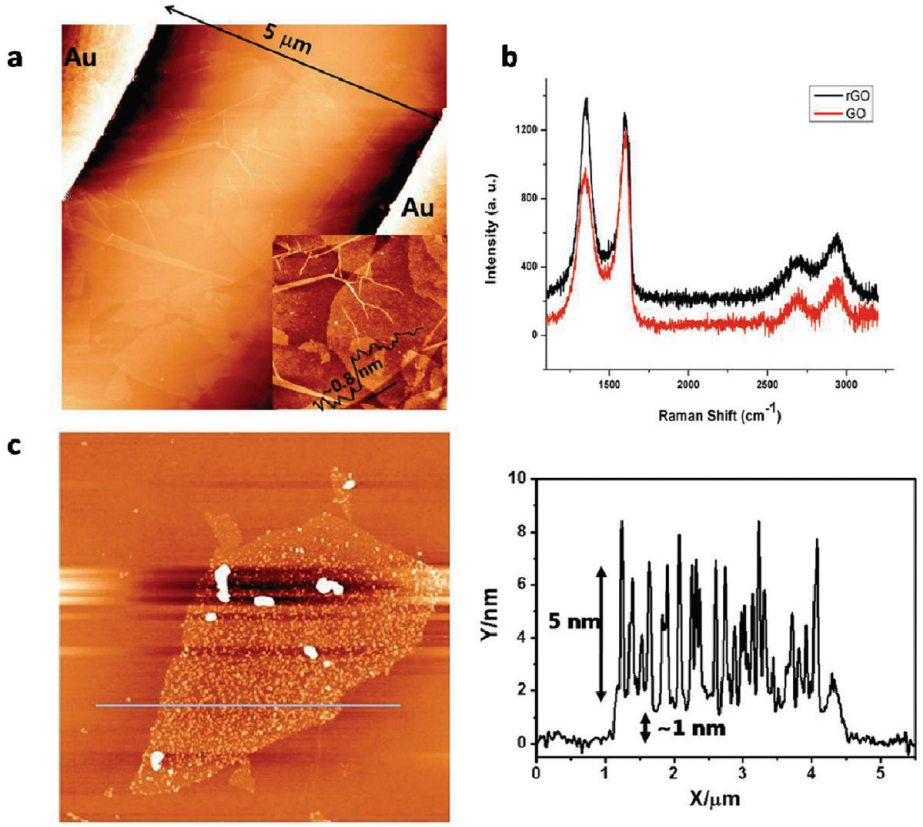

Figure 3. (a) Topographical AFM image of rGO sheets deposited onto the SiO_2 between an Au source-electrode (left) and an Au drain-electrode (right) device (inset: a cross-sectional analysis of a single rGO sheet). The rGO single layers were overlapped, single layer by single layer, to form a channel between two gold electrodes with a gap width of 5 μm. (b) Raman Spectra of rGO sheets from the rGO device (black) and GO sheets from a GO device (red). The D and G peaks corresponding to vibrations of sp^2 carbon were observed at 1350 and 1600 cm^{-1}, respectively, in both the rGO and GO devices. With the chemical reduction by hydrazine vapor, the intensity ratio of the D and G peaks (I(D)/I(G): 1.07) in the rGO device increased significantly compared with the ratio (I(D)/I(G): 0.80) in the GO device, revealing that some oxygen groups on the rGO were removed, resulting in defects. (c) Topographical AFM image (7.1 × 7.1 μm^2) of AuNP-frGO on a SiO_2 substrate. The cross-sectional analysis of a single AuNPs-frGO sheet indicates that AuNPs (5 nm) were successfully immobilized on the rGO sheet by the MBDT linkers.

of the hydroxyl and carboxylic acid groups of GO. The transfer curve (showing the drain-source electrode current as a function of gate voltage, $I_{ds}-V_g$) of the bare rGO device was ambipolar and had a low current range from 1×10^{-6} to 1×10^{-9} ampere, indicating the semiconducting property of this channel (Figure S1, Supporting Information).

Furthermore, after functionalization of the rGOs with MBDT molecules, the C−C peak showed a positive shift of approximately 0.2 eV to 284.639 eV in the XPS spectrum of the MBDT functionlized rGO (Figure 2b), which indicated the presence of new sp^3 C−C bonds owing to the bonding of MBDT molecules to rGOs.[26] A significant amount (about 7%) of sulfur was detected (Figure 2d), indicating that the rGO surface had successfully functionalized with diazotized MBDT molecules, generating new C−C covalent bonds.[26] Figure 2e shows the XPS spectrum of the AuNP-frGO sample in the S2p region, confirming the chemical binding between the AuNP and the frGO. The binding energy of S2p around 164 eV[27] was attributed to the unbound thiol groups on the frGO (Figure 2d), and as the AuNPs immobilized on the frGO *via* thiol linkers, the peak intensity of the exposed terminal sulfur at 164 eV decreased dramatically. A new peak appeared at 162.2 eV,[27] which was an S2p binding energy attributed to the bound sulfur on the AuNPs (Figure 2e). These results are consistent with previous studies,[27−29] confirming the formation of covalent bonds between gold and sulfur (*i.e.,* AuNPs-MBDT frGO). Furthermore, the Au4f peak in the AuNP-frGO sample was observed at both 84.4 and 88.4 eV by XPS (Figure 2f), indicating that AuNPs were bound to frGOs with molecular linkers.[30] Consequently, the XPS data proved that AuNPs were successfully bound to rGOs with chemical bonds by the thiol groups of the bifunctionalized MBDT molecules. A topographical AFM image (Figure 3c) also confirmed that AuNPs were well-attached onto the frGO sheet; the cross-sectional analysis showed ~5 nm AuNPs on a ~1 nm frGO sheet.

Figure 4a shows the $I-V$ curves obtained from the AuNP-frGO horizontal device. The sample was tested in vacuum (10^{-4} Torr) conditions. The $I-V$ characteristics

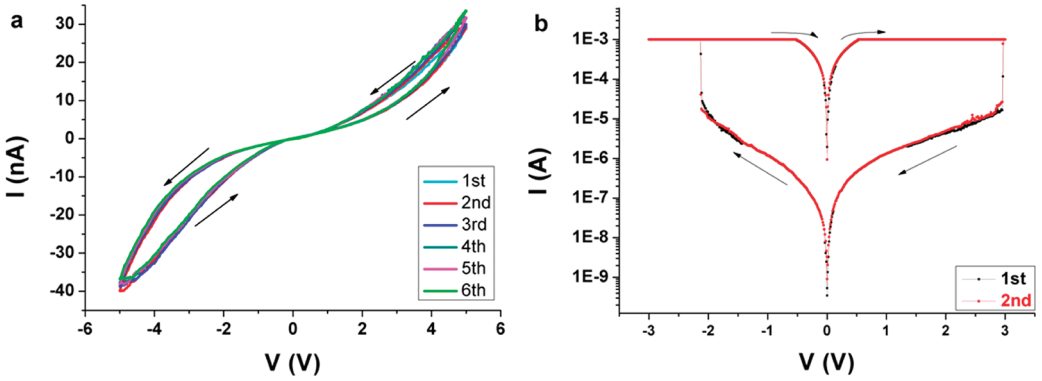

Figure 4. (a) *I*−*V* characteristics on linear scales of the horizontal AuNPs-frGO device (*i.e.*, Au source-electrode/AuNP-frGO/Au drain-electrode) and (b) *I*−*V* characteristics on log scales of the vertical device (*i.e.*, Al top-electrode/AuNP-frGOs hybrid material film/ITO bottom-electrode). Noticeable nonlinear hysteresis is observed in all devices.

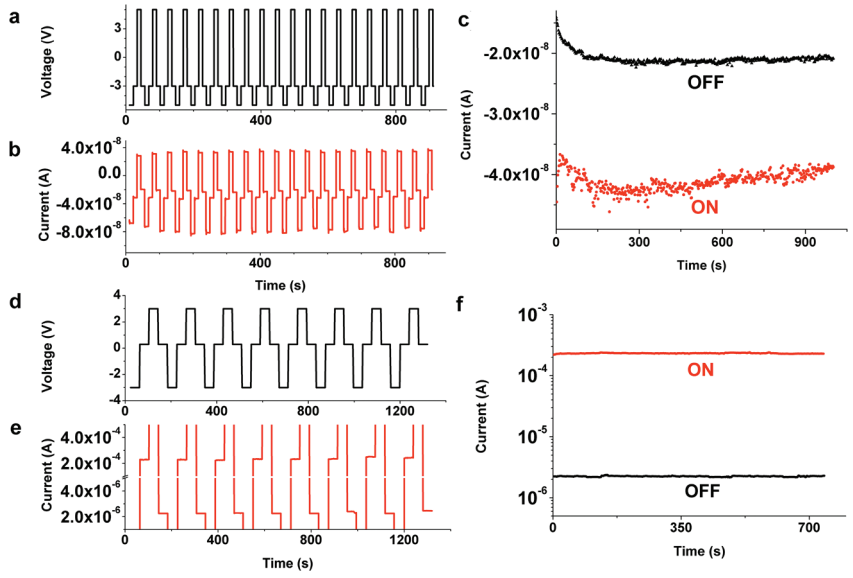

Figure 5. Write−multiple read−erase−multiple read (WRER) cycles and retention times of an AuNP-frGO device. (a) Input and (b) output of the WRER cycles of a horizontal device, for rewritable data storage applications. Voltage: W, −5.0; R, −3.0; E, +5.0; and R, −3.0 V. (c) Retention times for the ON and OFF states of the horizontal device, probed with voltages at −3.0 V. The ON and OFF states were induced by pulses of −5.0 and +5.0 V, respectively. (d) Input and (e) output of the WRER cycles of a vertical device, for rewritable data storage applications. Voltage: W, −3.0; R, 0.3; E, +3.0; and R, 0.3 V. (f) Retention times for the ON and OFF states of the vertical device, probed with a voltage of 0.3 V. The ON and OFF states were induced by pulses of −3.0 and +3.0 V, respectively.

of the device were measured by scanning applied voltages from 0 to −5 V, from −5 V to +5 V, and then back to 0 V in a cycle. The scanning speed was 9.6 s/V and the current error ranges were ±5 nA. The *I*−*V* curves were consistently reproducible and showed nonlinear hysteresis behavior. As shown in Figure 4a, the stable current hysteresis was sustained during continuous voltage sweeps. The current hysteresis behavior of the device could be exploited as a switch or memory, depending on the retention time.[31,32] On the other hand, a control experiment was also done with a blank device that did not contain any AuNPs. No hysteresis loop was observed in the *I*−*V* curves of this device (Figure S2, Supporting Information). In addition, when AuNPs without the MBDT molecular linker were used, no large hysteresis effect was observed (Figure S3, Supporting Information), which was prepared by direct immersion of the rGO device into a gold colloid solution. Consequently, the *I*−*V* curves in Figure 4a reveal that the current hysteresis of the AuNPs-frGO device clearly originate from the AuNPs covalently bound to the frGO.

For proving the thickness effect of the active AuNP-frGOs layer on the memory device performance, we also fabricated a vertical device with a sandwich structure between two metal electrodes (*i.e.*, Al/AuNP-frGOs/ITO). For the AuNP-frGO vertical device depicted in Figure 4b, the ON/OFF ratios sharply increased with an increase in AuNP-frGO film thickness. The *I*−*V* curves of the AuNP-frGO vertical device were dipolar, stable, and reproducible. The ON/OFF ratio was about 100 with a 50-nm AuNP-frGOs film thickness. These were recorded by scanning the applied voltage from 0 to −3 V initially,

then ramping up to +3 V, followed by a reverse scan from +3 to 0 V. Note that the positive bias corresponds to a positive voltage applied to the top metal pad, whereas a negative bias corresponds to a negative voltage applied to the top pad. On the other hand, since only the monolayer of AuNPs was employed, the ON/OFF ratio of AuNPs-frGO horizontal device was 2 (Figure 4a), which is relatively small compared to the thick-film memory devices including the AuNP-frGO vertical device (Figure 4b).[31] However, a small ON/OFF ratio with a low driving voltage is desirable in the fields of nanoscaled molecular electronics.[32,33] For example, devices with small ON/OFF ratios can be used as random-access memory devices.[32] According to previous reports, the retention time of the ON- and OFF-current states is a critical determinant of whether the device can be used as a volatile or nonvolatile memory device.[31]

To determine whether the AuNP-frGO device possessed sufficient stability for use as a memory device, its current responses to write−multiple read−erase−multiple read (WRER) cycles were tested for each operational voltage (Figure 5). For the horizontal device, the write and erase operations were performed at a voltage of −5 and +5 V, respectively, and the read cycle occurred at −3 V (Figure 5a). The ON and OFF states emerged repeatedly when the bias voltage was changed from the writing (−5 V) or erasing (+5 V) voltage to the reading (−3 V) voltage (Figure 5b). Performances of WRER cycles were notably stable when compared to the previous thin-film or monolayer memory devices. Figure 5c showed plots of current *versus* time for AuNP-frGO horizontal device in both the ON (red) and OFF (black) states. The ON (OFF) state was pulsed with a write (erase) voltage at −5 V (+5 V) for 10 s and then programmed with a read voltage at −3 V. After pulsing the write (erase) voltage, neither the ON nor the OFF state decayed; these states were maintained for more than 1000 s. Furthermore, the retention times of the ON and OFF states were greater than 1000 s without significant enervation, indicating that the AuNP-frGO device can, in fact, be used as a nonvolatile memory device.[31] In addition to the excellent memory performance of the horizontal device, the vertical device also exhibited stable memory performances: WRER cycles were found to be stable over 1200 s (Figure 5d,e) and a long retention time of over 700 s (Figure 5f) was shown, which indicate the stable conducting switching behavior of the AuNP-frGO vertical device.

On the basis of the results from our control experiments (*e.g.*, chemically functionalized rGO devices with MBDT but without AuNPs, and physically immobilized rGO devices with AuNPs but without MBDT linkers), the charging effect that caused the AuNPs-frGO device to operate with nonvolatile memory behavior can be associated with the AuNPs connected to rGOs by MBDT linkers.[34,35] In general, the charged state of AuNPs may lead to a space-charge field that prevents or accelerates carrier transport. Then, the field distribution of the rGO layers may fluctuate owing to the transport of moving carriers charged by AuNPs *via* MBDT molecular linkers. Thus, AuNPs acting as capacitors can charge and discharge moving carriers depending on the bias voltage applied between the two electrodes.[36−38] Presumably, the high potential barrier is caused by the large difference in potential energy between the lowest unoccupied molecular orbital (LUMO) level of the rGO and the work function of the AuNPs.[39] In fact, use of a molecular linker between the rGO and the AuNPs was expected to provide a larger potential barrier than that from direct contact of AuNPs embedded in an organic layer.[17,36] Because of the large energy barrier between the AuNPs and the rGO channel, the AuNPs can access the electrons when a bias voltage is applied to an AuNP-frGO device, causing them to become trapped inside the AuNPs. Consequently, these trapped electron carriers can remain inside the AuNPs for a relatively long time, even after the applied bias has been removed, resulting in a remarkable nonvolatile memory effect for both horizontal and vertical nanoscaled thin-film AuNP-frGO devices.

CONCLUSIONS

We have successfully fabricated AuNP-frGO nonvolatile memory devices with both horizontal and vertical structures. The horizontal memory device consisted of monolayered AuNPs and a thin-film rGO semiconducting channel that were linked by bifunctional molecules. The semiconducting transport channel in the AuNPs-frGO device was constructed of singly or doubly overlayered rGOs. By comparison to the control experiments, the horizontal single-layered AuNP-frGO device clearly demonstrated that the charging effect originates from the AuNPs covalently bound to the frGO. The *I*−*V* characteristics of both horizontal and vertical AuNP-frGO devices showed a reproducible and noticeable nonlinear hysteresis, stable write−multiple read−erase−multiple read cycles over 1000 s, and a long retention time of more than 700 s. The vertical AuNP-frGO memory devices showed a large current ON/OFF ratio and high stability, making them potentially applicable in nonvolatile memory electronics.

MATERIALS AND METHODS

Synthesis of 4-Mercapto-benzenediazonium Tetrafluoroborate (MBDT) Salt. In a flask, 4-aminothiophenol was dissolved in ethanol, and an aqueous fluoroboric acid (48% solution) was added to the flask. The mixture was then cooled to −5 °C. Isoamyl nitrite was added dropwise to the mixture and then the mixture was stirred for 0.5 h. The mixture was then diluted with diethyl ether, which resulted in the precipitation of MBDT as brown crystals. MBDT

was purified by recrystallization using acetone and cold diethyl ether, respectively. Chemical characterization was performed by ^{1}H NMR and FT-IR spectra (see Supporting Information for NMR and FT-IR data).

Preparation of the GO Solution. Graphene oxide was synthesized using a modified Hummer's method. A 40 mg portion of GO and 40 mL of deionized (DI) water were mixed together in a falcon-tube. To disperse GO in the DI water, sonication for more than 2 h (using a Branson ultrasonicator) was necessary. The GO solution was shaken at 200 rpm for 1 h, centrifuged at 500 rpm for 1.5 h, and then left standing for 2 h. The supernatant was then removed and stored until needed for further experimentation. Before use, the supernatant of the GO solution was sonicated for 1 h, shaken at 200 rpm for 1 h, and left standing for 2 h.

Fabrication of the Horizontal Device. An electrode-fabricated device was chemically cleaned using a piranha solution, which is a mixture of H_2O_2 and H_2SO_4 (note: handle with careful caution). The device was then washed with DI water several times. Using a microsyringe, the GO solution was spin-casted onto the device at 4000 rpm. The GO device was dried for 24 h under vacuum conditions. Then, the GO device was placed on the top of a carrier in a glass chamber and hydrazine monohydrate was dropped into the chamber. After sealing the chamber, the whole system was heated at 80 °C for 24 h, and the hydrazine was vaporized to reduce GO into rGO. After reduction, an MBDT solution in acetonitrile (ACN) was prepared at a concentration of 70 mM. Then, the rGO device was immersed in the solution for 24 h. (All steps were performed in a glovebox.) The frGO device was washed thoroughly with ACN and acetone (both HPLC grade) and blown with nitrogen gas to remove the solvent. The frGO device was kept in a vacuum before use. For the immobilization of the AuNPs, the frGO device was placed into a gold colloid solution for 120 h, then washed with DI water and blown dry with nitrogen gas. The AuNP-frGO device was then kept in a vacuum.

Fabrication of the Vertical Device. (1) Synthesis of the AuNP-frGO: Chemical reduction was carried out by adding 30 μL of hydrazine monohydrate to a 30-mL GO solution (1 mg·mL^{-1}). The reaction mixture was heated at 95 °C for 1 h. After cooling to room temperature, the predissolved MBDT aqueous solution was added dropwise to the rGO solution while stirring. Next, a 3-mL gold colloid solution was added, and the reaction contents were allowed to stir for 1 h at room temperature. The mixture was then filtered through a 0.45 μm PTFE membrane, washed with water and acetone (3 times), and resuspended in DMF to remove the excess diazonium salt. This process was followed by filtration (a 0.45 μm PTFE membrane) and copious washing of the filter cake with acetone. The resulting solid was dried at 80 °C in a vacuum oven overnight yielding the AuNP-frGO. For the control experiment, the gold colloid solution was not used so that only frGO was prepared. (2) Preparation of the ITO/AuNP-frGO/Al device: The ITO glass bottom electrode was cleaned by sonication with acetone and ethanol, and then was washed several times with deionized water and ethanol. Finally, it was dried under a stream of nitrogen gas. For fabrication of the vertical device, AuNP-frGO (frGO as control) in DMF solution was spun onto the ITO electrode at 200 rpm for 15 s, followed by 1250 rpm for 45 s. The final speed was 2500 rpm for 20 s. Then the thin film was dried in a vacuum at room temperature overnight. An aluminum top-electrode (200 nm thick) was evaporated through a shadow mask onto the AuNP-frGO surface using an electron beam evaporator under 5.0×10^{-7} Torr.

Surface and Electrical Characterization. Atomic force microscopy (SPA 3800, Seiko), Raman spectroscopy (Reinshaw, RM1000-In Via), and XPS (VG microtech ESCA 2000) were used for surface characterization. A 4200 Keithley semiconductor characterization system was used for measurements of the electrical properties of the device.

Acknowledgment. This work was supported by the Creative Research Initiatives research fund (project title: Smart Molecular Memory) of MEST/NRF.

Supporting Information Available: Additional *I*–*V* characteristics and additional characterizations of the MBDT. This material is available free of charge via the Internet at http://pubs.acs.org.

REFERENCES AND NOTES

1. Novoselov, K. S.; Geim, A. K.; Morozov, S. V.; Jiang, D.; Katsnelson, M. I.; Grigorieva, I. V.; Dubonos, S. V.; Firsov, A. A. Two-Dimensional Gas of Massless Dirac Fermions in Graphene. *Nature* **2005**, *438*, 197–200.
2. Li, X.; Wang, X.; Zhang, L.; Lee, S.; Dai, H. Chemically Derived, Ultrasmooth Graphene Nanoribbon Semiconductors. *Science* **2008**, *319*, 1229–1232.
3. Geim, A. K.; Novoselov, K. S. The Rise of Graphene. *Nat. Mater.* **2007**, *6*, 183–191.
4. Blake, P.; Brimicombe, P. D.; Nair, R. R.; Booth, T. J.; Jiang, D.; Schedin, F.; Ponomarenko, L. A.; Morozov, S. V.; Gleeson, H. F.; Hill, E. W.; Geim, A. K.; Novoselov, K. S. Graphene-Based Liquid Crystal Device. *Nano Lett.* **2008**, *8*, 1704–1708.
5. Wang, X.; Zhi, L.; Mullen, K. Transparent, Conductive Graphene Electrodes for Dye-Sensitized Solar Cells. *Nano Lett.* **2008**, *8*, 323–327.
6. Du, X.; Skachko, I.; Barker, A.; Andrei, E. Y. Approaching Ballistic Transport in Suspended Graphene. *Nat. Nanotechnol.* **2008**, *3*, 491–495.
7. Morozov, S. V.; Novoselov, K. S.; Katsnelson, M. I.; Schedin, F.; Elias, D. C.; Jaszczak, J. A.; Geim, A. K. Giant Intrinsic Carrier Mobilities in Graphene and Its Bilayer. *Phys. Rev. Lett.* **2008**, *100*, 016602.
8. Bolotin, K. I.; Sikes, K. J.; Jiang, Z.; Klima, M.; Fudenberg, G.; Hone, J.; Kim, P.; Stormer, H. L. Ultrahigh Electron Mobility in Suspended Graphene. *Sol. State Commun.* **2008**, *146*, 351–355.
9. Hummers, W. S.; Offeman, R. E. Preparation of Graphitic Oxide. *J. Am. Chem. Soc.* **1958**, *80*, 1339–1339.
10. Cote, L. J.; Kim, F.; Huang, J. Langmuir–Blodgett Assembly of Graphite Oxide Single Layers. *J. Am. Chem. Soc.* **2008**, *131*, 1043–1049.
11. Marcano, D. C.; Kosynkin, D. V.; Berlin, J. M.; Sinitskii, A.; Sun, Z.; Slesarev, A.; Alemany, L. B.; Lu, W.; Tour, J. M. Improved Synthesis of Graphene Oxide. *ACS Nano* **2010**, *4*, 4806–4814.
12. Moon, I. K.; Lee, J.; Ruoff, R. S.; Lee, H. Reduced Graphene Oxide by Chemical Graphitization. *Nat. Commun.* **2010**, *1*, 73.
13. Dreyer, D. R.; Murali, S.; Zhu, Y.; Ruoff, R. S.; Bielawski, C. W. Reduction of Graphite Oxide Using Alcohols. *J. Mater. Chem.* **2011**, *21*, 3443–3447.
14. Gilje, S.; Han, S.; Wang, M.; Wang, K. L.; Kaner, R. B. A Chemical Route to Graphene for Device Applications. *Nano Lett.* **2007**, *7*, 3394–3398.
15. Eda, G.; Fanchini, G.; Chhowalla, M. Large-Area Ultrathin Films of Reduced Graphene Oxide as a Transparent and Flexible Electronic Material. *Nat. Nanotechnol.* **2008**, *3*, 270–274.
16. Myung, S.; Park, J.; Lee, H.; Kim, K. S.; Hong, S. Ambipolar Memory Devices Based on Reduced Graphene Oxide and Nanoparticles. *Adv. Mater.* **2010**, *22*, 2045–2049.
17. Leong, W. L.; Mathews, N.; Mhaisalkar, S. G.; Chen, T. P.; Lee, P. S. Charging Dynamics of Discrete Gold Nanoparticle Arrays Self-Assembled within a Poly(styrene-b-4-vinylpyridine) Diblock Copolymer Template. *Appl. Phys. Lett.* **2008**, *93*, 222908.
18. Bozano, L. D.; Kean, B. W.; Beinhoff, M.; Carter, K. R.; Rice, P. M.; Scott, J. C. Organic Materials and Thin-Film Structures for Cross-Point Memory Cells Based on Trapping in Metallic Nanoparticles. *Adv. Funct. Mater.* **2005**, *15*, 1933–1939.
19. Wilson, N. R.; Pandey, P. A.; Beanland, R.; Young, R. J.; Kinloch, I. A.; Gong, L.; Liu, Z.; Suenaga, K.; Rourke, J. P.; York, S. J.; Sloan, J. Graphene Oxide: Structural Analysis and Application as a Highly Transparent Support for Electron Microscopy. *ACS Nano* **2009**, *3*, 2547–2556.
20. Stankovich, S.; Dikin, D. A.; Piner, R. D.; Kohlhaas, K. A.; Kleinhammes, A.; Jia, Y.; Wu, Y.; Nguyen, S. T.; Ruoff, R. S. Synthesis of Graphene-Based Nanosheets *via* Chemical Reduction of Exfoliated Graphite Oxide. *Carbon* **2007**, *45*, 1558–1565.
21. Zhou, M.; Zhai, Y.; Dong, S. Electrochemical Sensing and Biosensing Platform Based on Chemically Reduced Graphene Oxide. *Anal. Chem.* **2009**, *81*, 5603–5613.

22. Park, S.; An, J.; Jung, I.; Piner, R. D.; An, S. J.; Li, X.; Velamakanni, A.; Ruoff, R. S. Colloidal Suspensions of Highly Reduced Graphene Oxide in a Wide Variety of Organic Solvents. *Nano Lett.* **2009**, *9*, 1593–1597.
23. Eda, G.; Chhowalla, M. Chemically Derived Graphene Oxide: Towards Large-Area Thin-Film Electronics and Optoelectronics. *Adv. Mater.* **2010**, *22*, 2392–2415.
24. Tuinstra, F.; Koenig, J. L. Raman Spectrum of Graphite. *J. Chem. Phys.* **1970**, *53*, 1126–1130.
25. Rao, C. N. R.; Sood, A. K.; Subrahmanyam, K. S.; Govindaraj, A. Graphene: The New Two-Dimensional Nanomaterial. *Angew. Chem., In. Ed.* **2009**, *48*, 7752–7777.
26. Zhu, Y.; Higginbotham, A. L.; Tour, J. M. Covalent Functionalization of Surfactant-Wrapped Graphene Nanoribbons. *Chem. Mater.* **2009**, *21*, 5284–5291.
27. Zhang, S.; Leem, G.; Srisombat, L.-o.; Lee, T. R. Rationally Designed Ligands that Inhibit the Aggregation of Large Gold Nanoparticles in Solution. *J. Am. Chem. Soc.* **2007**, *130*, 113–120.
28. Bang, G. S.; Park, J.; Lee, J.; Choi, N.-J.; Baek, H. Y.; Lee, H. Rose Bengal Dye on Thiol-Terminated Bilayer for Molecular Devices. *Langmuir* **2007**, *23*, 5195–5199.
29. Bang, G. S.; Chang, H.; Koo, J.-R.; Lee, T.; Advincula, R. C.; Lee, H. High-Fidelity Formation of a Molecular-Junction Device Using a Thickness-Controlled Bilayer Architecture. *Small* **2008**, *4*, 1399–1405.
30. Harnisch, J. A.; Pris, A. D.; Porter, M. D. Attachment of Gold Nanoparticles to Glassy Carbon Electrodes *via* a Mercaptobenzene Film. *J. Am. Chem. Soc.* **2001**, *123*, 5829–5830.
31. Lee, J.; Chang, H.; Kim, S.; Bang, G. S.; Lee, H. Molecular Monolayer Nonvolatile Memory with Tunable Molecules. *Angew. Chem. In. Ed.* **2009**, *48*, 8501–8504.
32. Kim, H. J.; Jeong, W. C.; Koh, K. H.; Jeong, G. T.; Park, J. H.; Lee, S. Y.; Oh, J. H.; Song, I. H.; Jeong, H. S.; Kinam, K. A Process Integration of High-performance 64-kb MRAM. *IEEE Trans. Magn.* **2003**, *39*, 2851–2853.
33. He, J.; Chen, B.; Flatt, A. K.; Stephenson, J. J.; Doyle, C. D.; Tour, J. M. Metal-free Silicon-Molecule-Nanotube Testbed and Memory Device. *Nat. Mater.* **2006**, *5*, 63–68.
34. Tondelier, D.; Lmimouni, K.; Vuillaume, D.; Fery, C.; Haas, G. Metal/Organic/Metal Bistable Memory Devices. *Appl. Phys. Lett.* **2004**, *85*, 5763–5765.
35. Kano, M.; Orito, S.; Tsuruoka, Y.; Ueno, N. Nonvolatile Memory Effect of an Al/2-Amino-4,5-dicyanoimidazole/Al Structure. *Synth. Metal.* **2005**, *153*, 265–268.
36. Wang, H. P.; Pigeon, S.; Izquierdo, R.; Martel, R. Electrical Bistability by Self-Assembled Gold Nanoparticles in Organic Diodes. *Appl. Phys. Lett.* **2006**, *89*, 183502–3.
37. Bozano, L. D.; Kean, B. W.; Deline, V. R.; Salem, J. R.; Scott, J. C. Mechanism for Bistability in Organic Memory Elements. *Appl. Phys. Lett.* **2004**, *84*, 607–609.
38. Simmons, J. G.; Verderber, R. R. New Conduction and Reversible Memory Phenomena in Thin Insulating Films. *Proc. R. Soc. Lond. A* **1967**, *301*, 77–102.
39. Kong, B.-S.; Geng, J.; Jung, H.-T. Layer-by-Layer Assembly of Graphene and Gold Nanoparticles by Vacuum Filtration and Spontaneous Reduction of Gold Ions. *Chem. Commun.* **2009**, 2174–2176.